

# Study on the interactive deformation of bone needles and circum-pelvic soft tissue<sup>①</sup>

ZHANG Famin (张发敏)<sup>\*</sup>, LEI Jingtao<sup>②</sup> \* \*\*

(<sup>\*</sup> School of Mechatronic Engineering and Automation, Shanghai University, Shanghai 200444, P. R. China)

(<sup>\*\*</sup> Shanghai Key Laboratory of Intelligent Manufacturing and Robotics, Shanghai 200444 P. R. China)

## Abstract

During the robot-assisted pelvic fracture reduction, the needle-tissue interactive deformation characteristic is not clear, which affects the accuracy of robotic surgery. In this paper, a layered rigid-flexible coupling model is proposed, and the needle-tissue interactive deformation under the loading is analyzed by the Rayleigh-Ritz method, in accordance with the principle of minimum potential energy. The pelvic musculoskeletal tissue is reversely reconstructed, and the structure of the bone is segmented into cancellous bone and cortical bone. The Mooney-Rivlin five-parameter hyperelastic model is used to simulate muscle, and the Ogden hyperelastic model is used to simulate adipose tissue. Finite element simulation is performed by loading different magnitudes of forces. The accuracy of the rigid-flexible coupling model is 0.432 mm, which indicates the correctness of the needle-tissue interactive deformation theory analysis.

**Key words:** pelvic fracture reduction, rigid-flexible coupling, needle-tissue interactive deformation

## 0 Introduction

Pelvic fracture is a common injury. Before robot-assisted pelvic fracture reduction, multiple bone needles need to be inserted into the pelvic bone. The needles are held through the clamping device, which is also connected to the robot. Under the influence of the reduction force, both the circum-pelvic soft tissue and bone needles are susceptible to uneven deformation or stress concentration, directly affect the precision of reduction surgery. Therefore, it is necessary to establish a refined rigid-flexible coupling model between bone needles and pelvic soft tissue for analyzing the deformation characteristics during their interaction.

Many scholars have studied the deformation of rigid-flexible coupling tissue. Ref. [1] discretized tissues into grid nodes and employed the finite element method to fit the trajectory of needle deflection in the plane. Refs [2, 3] characterized the interaction between the needle and soft tissue as a series of linear springs with constant stiffness, using the Euler-Bernoulli beam theory to estimate the deformation of the puncture needle in soft tissue. Refs [4, 5] employed a series of Kelvin-Voigt viscoelastic models to simulate

tissue forces along the needle cutting path. Ref. [6] utilized a spring-damping model to simulate the mechanical properties of soft tissue. Ref. [7] decomposed tissue deformation into a mass-spring-damping system, and established the stiffness matrix for the system. Ref. [8] improved the Euler-Bernoulli beam theory and established a coupled model for needle penetration through multiple layers of tissue. Ref. [9] proposed a virtual spring-supported cantilever beam model and employed the Rayleigh-Ritz method to predict the trajectory of needle puncture. Ref. [10] employed a coupled Euler-Lagrangian finite element method to simulate the penetration of a flexible needle through multiple layers of pig liver tissue. Ref. [11] employed an energy-based approach, decomposed the energy during the needle insertion process into bending energy, deformation energy and work done in needle-tissue interaction.

Although many scholars have carried out research on the mechanical model of soft tissue and the finite element analysis of soft tissue deformation, there is no report on the interactive deformation of bone needles and pelvic soft tissue under the action of large reduction force during the reduction of pelvic fracture. Most

① Supported by the National Key R&D Program of China (No. 2020YFB1313803).

② To whom correspondence should be addressed. E-mail: jtlei2000@163.com.

Received on Jan. 10, 2024

previous studies used single-layer soft tissue models.

Aiming at the unclear characteristic of needle-tissue interactive deformation during the robot pelvic fracture reduction, a kind of layered rigid-flexible coupling is presented, and force analysis is carried out. The Rayleigh-Ritz method is used to analyze the deformation of needles. Based on the computer tomography (CT) data of the patient's injured pelvis, the model of the pelvis and soft tissue is reversely reconstructed. The interactive deformation of needle-tissue is simulated by applying forces of 100 N, 200 N and 300 N to verify the correctness of the proposed rigid-flexible coupling model deformation theory analysis.

## 1 Pelvic soft tissue modeling

### 1.1 Reconstruction of pelvic soft tissue

According to anatomical principles, the tissue that the bone needles pass through are the skin, adipose tissue, muscles and bones, as shown in Fig. 1.

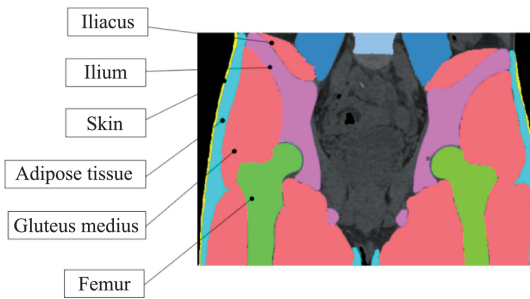


Fig. 1 MRI of pelvic soft tissue

The patient's pelvic CT data is imported into the medical image processing software Mimics, and a three-dimensional model of the pelvic skeleton and muscles is reverse-reconstructed. The model is subjected to optimization processes, including noise reduction and surface smoothing, using Geomagic software. Finally, the pelvic skeleton and muscles are assembled by using SolidWorks to obtain the 3D model of the pelvic bone and muscles, as shown in Fig. 2.

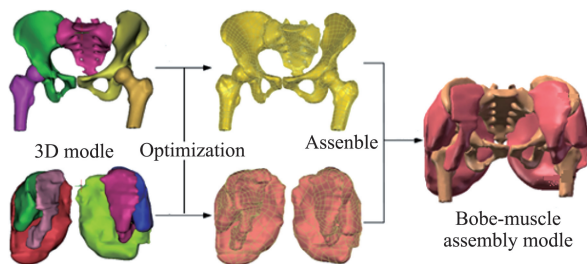


Fig. 2 Reconstruction of 3D model

The human bones can be structurally categorized into cortical bone and cancellous bone. Cortical bone has a higher bone density. The trabecular arrangement of cancellous bone is loose, and the texture is relatively soft. The bone separation is carried out through Boolean operations, which can more accurately reflect the characteristics of human bones. The 3D model of adipose tissue is generated through operations such as extracting muscle and skeletal surfaces, thickening, and other processes, as shown in Fig. 3.

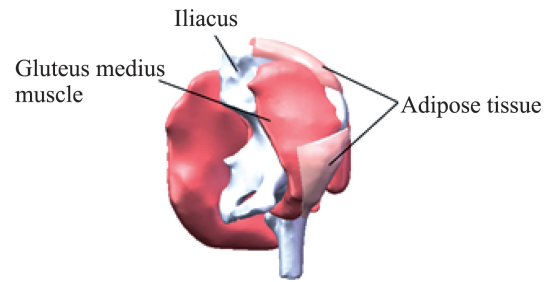


Fig. 3 3D model of adipose tissue

### 1.2 Biomechanical modeling of soft tissue

#### 1.2.1 Muscle tissue

In this paper, the Mooney-Rivlin five-parameter model is used as the constitutive model of muscle for modeling and simulation. The general form of the strain energy function of the Mooney-Rivlin model is as follows.

$$W = (C_{10} + C_{01})(I_1 - 3) + C_{20}(I_1 - 3)^2 + (C_{11} + C_{02})(I_1 - 3)^3 \quad (1)$$

where,  $C_{10}$ ,  $C_{01}$ ,  $C_{20}$ ,  $C_{11}$ ,  $C_{02}$  are material characteristic parameters,  $W$  is the strain energy function, and  $I_1$  is the first invariant of the Cauchy tensor.

Under uniaxial quasi-static compression, the stress in the loading direction is as follows.

$$\sigma_1^e = 2(\lambda^2 - \lambda^{-1})[C_{10} + C_{01} + 2] + 2(C_{11} + C_{02} + C_{20})(\lambda^2 + 2\lambda^{-1} - 3) \quad (2)$$

where  $\lambda$  is the elongation ratio, and the relationship between  $\lambda$  and strain  $\varepsilon$  is  $\lambda = 1 + \varepsilon$ .

The determination of the five Mooney-Rivlin parameters<sup>[12]</sup> is  $C_{10} = 0.08556$  MPa,  $C_{20} = 0.03900$  MPa,  $C_{01} = -0.05841$  MPa,  $C_{11} = -0.02320$  MPa,  $C_{02} = 0.00851$  MPa.

#### 1.2.2 Adipose tissue

Many studies have shown that the first-order Ogden hyperelastic material constitutive model performs well in simulating the mechanical properties of adipose

tissue.

The strain energy function of the first-order Ogden model can be defined as

$$W^{Ogdl} = \frac{u^{Ogdl}}{\alpha^{Ogdl}} (\lambda_1^{\alpha^{Ogdl}} + \lambda_2^{\alpha^{Ogdl}} + \lambda_3^{\alpha^{Ogdl}} - 3) + \frac{1}{d^{Ogdl}} (J - 1)^2 \quad (3)$$

where,  $\lambda_1, \lambda_2, \lambda_3$  are the stretch ratios in the three main directions;  $u^{Ogdl}, \alpha^{Ogdl}$  are constants for material shear behavior;  $d^{Ogdl}$  is compressibility; and  $J$  is the determinant of the elastic deformation gradient.

The deformation of incompressible materials satisfies the following constraints:

$$J = \lambda_1 \lambda_2 \lambda_3 = 1 \quad (4)$$

Under uniaxial tensile load, the stretch ratio in the main direction is  $\lambda_U = \lambda_1$ , and the ratio in other directions is

$$\lambda_U^{-0.5} = \lambda_2 = \lambda_3 \quad (5)$$

The stretch ratio  $\lambda_i$  and strain  $\varepsilon_i$  also satisfy the following relationship:

$$\lambda_i = \varepsilon_i + 1 \quad (6)$$

Jebur et al. [13] conducted a stress-strain test and used Abaqus TM software to obtain the stress equation in the loading direction:

$$\sigma_U = \frac{2 u^{Ogdl}}{\alpha^{Ogdl}} (\lambda_U^{\alpha^{Ogdl}-1} - \lambda_U^{-\frac{1}{2}\alpha^{Ogdl}-1}) \quad (7)$$

Al-Dirini et al. [14] performed stress-strain curve fitting on quasi-static tensile tests on circum-pelvic fat samples and obtained Ogden's material parameters as  $\mu = 1.1667 \times 10^{-3}$  MPa,  $\alpha = 16.2, \rho = 0.92 \text{ g} \cdot \text{cm}^3$ .

## 2 Interactive deformation analysis

The reduction force output by the robot is transmitted from the bone needles to the affected side of the pelvis. Under the action of reduction force, the needle interacts with the soft tissue and deforms.

### 2.1 Rigid-flexible coupling model

Robot-assisted pelvic fracture reduction can be regarded as quasi-static. Considering the uneven characteristics of biological tissue, an interaction model of double-layer soft tissue and bone needles is proposed, as shown in Fig. 4. One end of the needle is fixed on the ilium, and the needle can be regarded as a slender cantilever beam. Due to the nonlinearity of the structure, each layer is modeled as a nonlinear spring with different stiffness and thickness.

The stiffness of lower soft tissue and upper soft tissue is  $k_1$  and  $k_2$  respectively. The relationship between the  $F(x)$  and the deformation  $x$  of a nonlinear

spring is shown in Eq. (8).

$$F(x) = k(x + x^3) \quad (8)$$

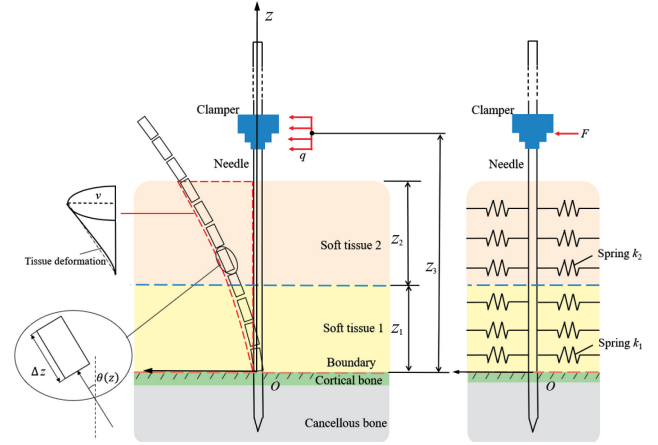


Fig. 4 Needle-tissue interaction model

### 2.2 Rayleigh-Ritz method

The Rayleigh-Ritz method [9] is an approximate solution to an unknown function. Based on the principle of minimum potential energy, the displacement that minimizes the total potential energy is the actual displacement of all possible displacements.

Firstly, the total potential energy of the needle-tissue system is calculated. And then a polynomial is chosen as the displacement equation for the bone needle. Lastly, the parameters in the displacement function are solved based on the condition of stationary values of potential energy.

The formula of calculating the potential energy of the needles-tissue interactive system is

$$\Pi_{\text{total}} = U_{\text{bend}} + U_{\text{interact}} - W_{\text{work}} \quad (9)$$

where,  $U_{\text{bend}}$  is the bending energy of the bone needles,  $U_{\text{interact}}$  is the mutual adhesion energy between the soft tissue and the bone needles, and  $W_{\text{work}}$  is the work done by the force acting on the bone needle.

(1) Bending deformation energy of bone needle

As the reduction force of pelvic fracture is large, so the needles will be bent and deformed. The bending deformation of bone needles  $U_{\text{bend}}$  is defined as

$$U_{\text{bend}} = \frac{EI}{2} \int_0^l \left( \frac{d^2 v(z)}{dz^2} \right)^2 dz \quad (10)$$

where,  $v(z)$  is the deflection of the bone needle,  $E$  is the elastic modulus of the bone needle,  $I$  is the second moment of the area, and  $l$  is the length of needle exposed outside the bone.

(2) Viscosity energy of pelvic soft tissue

The interaction between the bone needles and the soft tissue produces elastic potential energy, and the energy  $U_{\text{interact}}$  stored in the elastic medium is calculated

as follows.

$$\begin{aligned}
U_{\text{interact}} = & \sum_{z=0}^{Z_1} \frac{1}{2} k_1 \left( \frac{v(z)}{\cos(\theta(z))} \right)^2 \Delta z \\
& + \sum_{z=0}^{Z_1} \frac{1}{4} k_1 \left( \frac{v(z)}{\cos(\theta(z))} \right)^4 \Delta z \\
& + \sum_{z=Z_1}^{Z_1+Z_2} \frac{1}{2} k_2 \left( \frac{v(z)}{\cos(\theta(z))} \right)^2 \Delta z \\
& + \sum_{z=Z_1}^{Z_1+Z_2} \frac{1}{4} k_2 \left( \frac{v(z)}{\cos(\theta(z))} \right)^4 \Delta z
\end{aligned} \quad (11)$$

where,  $Z_1$  is the thickness of muscle tissue layer,  $Z_2$  is the thickness of adipose tissue layer, the stiffness of muscle tissue is  $k_1$ , the stiffness of adipose tissue is  $k_2$ , and  $\theta(z)$  is the deformation angle of the bone needle.

### (3) Work produced by applied load

The force exerted by the robot is uniformly distributed on the gripper, and the uniform load is  $q$ . The uniform load can be equivalently transformed into a concentrated load  $F$ , whose magnitude is the sum of the uniform load, and the action point is at the center of the uniform load. The work done by the force is

$$W_{\text{work}} = Fv(z_3) \quad (12)$$

where,  $v(z_3)$  is the deflection of the bone needle at the applied load.

A third-order polynomial is sufficient as the deformation curve of the bone needle.

$$v(z) = a_0 + a_1 z + a_2 z^2 + a_3 z^3 \quad (13)$$

The initial conditions are

$$v(0) = 0, \theta(0) = \frac{dv(0)}{dz} = 0 \quad (14)$$

According to the principle of minimum potential energy, the potential energy stationary condition is

$$\frac{\partial \Pi_{\text{total}}}{\partial a_j} = 0, j = 0, 1, 2, 3 \quad (15)$$

From Eq. (14),  $a_0 = a_1 = 0$  can be obtained.

According to Eq. (15), the parameters  $a_2$  and  $a_3$  can also be obtained, and the deformation of the bone needle can be solved.

## 2.3 Needle deformation

Song<sup>[15]</sup> randomly selected 10 adult patients with pelvic fracture in the hospital, and used postoperative CT to measure the average thickness of soft tissue with the result of  $31.82 \pm 5.43$  mm. According to the anatomical structure of the human body and Refs [16, 17], the biomechanical parameters of the double-layer soft tissue are set, as shown in Table 1.

According to Eqs (8) – (15) and the parameters of pelvic soft tissue and bone needle, the deformation curve of bone needle is obtained when  $F$  is 100 N,

200 N, and 300 N, as shown in Fig. 5.

Table 1 Soft tissue parameters

Parameter	Elastic modulus /MPa	Stiffness /( $\text{N} \cdot \text{mm}^{-1}$ )	Thickness /mm
Muscle tissue	$0.14 \times 10^6$	0.048	22
Adipose tissue	$0.06 \times 10^6$	0.023	10

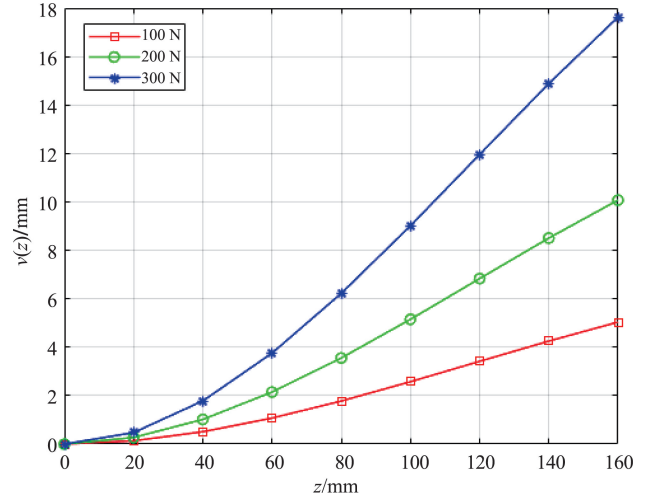


Fig. 5 Deformation of bone needle under different loads

It can be seen from Fig. 5 that the deformation of the bone needle exhibits a nonlinear trend. As the applied force increases, the deformation of the bone needle gradually increases. Under 300 N load, the deformation of the end of the bone needle is 17.63 mm, which increased by 250.08% compared with the deformation under 100 N load.

## 3 Simulation

### 3.1 Establishing a finite element model

The material of the gripper is defined as structural steel. The material parameters of pelvic bones and needles are shown in Table 2.

Table 2 Material parameters

Name	Elastic modulus /MPa	Density /( $\text{kg} \cdot \text{m}^{-3}$ )	Poisson ratio
Cortical bone	$1.70 \times 10^4$	$2.00 \times 10^3$	0.30
Cancellous bone	$1.50 \times 10^2$	$2.00 \times 10^3$	0.20
Bone needle	$1.10 \times 10^5$	$2.77 \times 10^3$	0.30
Clamper	$2.00 \times 10^5$	$7.85 \times 10^3$	0.30

The needles, clamper, and pelvic soft tissue are meshed with tetrahedron elements. The element length of the soft tissue model of the pelvis and the clamper is set to 3 mm, and the length of the needle unit is set to

1 mm. The element number of the model is 1 329 469, as shown in Fig. 6. Fixed constraints are added to the proximal femoral section, the superior surface of the sacrum, and the sacroiliac joint. The contact conditions between muscle and bone needle, as well as between muscle and bone, are set as ‘friction’, with a friction coefficient of 0.3. The friction coefficient between bone and bone needle is set to 0.9. The conditions of the remaining contact surfaces are set to ‘bonded’.

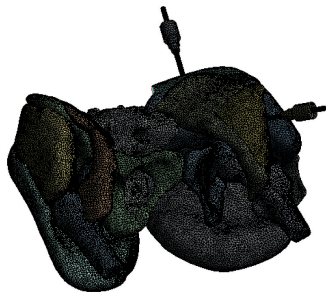


Fig. 6 Pelvic musculoskeletal model after meshing

### 3.2 Validation of biomechanical model

The bottom end of soft tissue is fixed as the boundary condition for traction, with the top of soft tissue as the traction site, as shown in Fig. 7. Displacements ranging from 0 to 10 mm are applied upward to the top of the iliacus muscle and adipose tissue. The stress-strain simulation curves for the iliacus muscle and adipose tissue are obtained and compared with the theoretical calculations from subsection 2.3, as shown in Fig. 8 and Fig. 9.

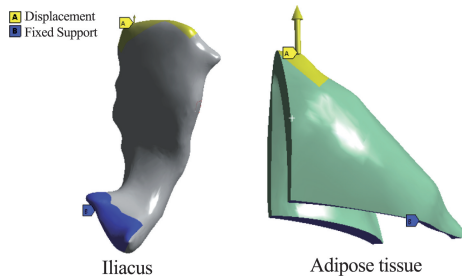


Fig. 7 Simulation of soft tissue traction

The root mean square error can be calculated according to the following formula:

$$RMSE = \sqrt{\frac{\sum_{i=1}^n (\sigma_{simu,i} - \sigma_{theo,i})^2}{n}} \quad (16)$$

where,  $\sigma_{simu}$  is the simulation stress value,  $\sigma_{theo}$  is the theoretical stress value,  $n$  is the amount of data.

The root mean square error (RMSE) between the

stress simulation value and the theoretical value of the iliacus muscle is 0.013 1, while that of the adipose is 0.010 5, both of which are less than 0.050 0. Comparing the stress-strain theoretical curve with the simulation curve, the trend and amplitude are basically consistent. It verifies the validity of the finite element model.

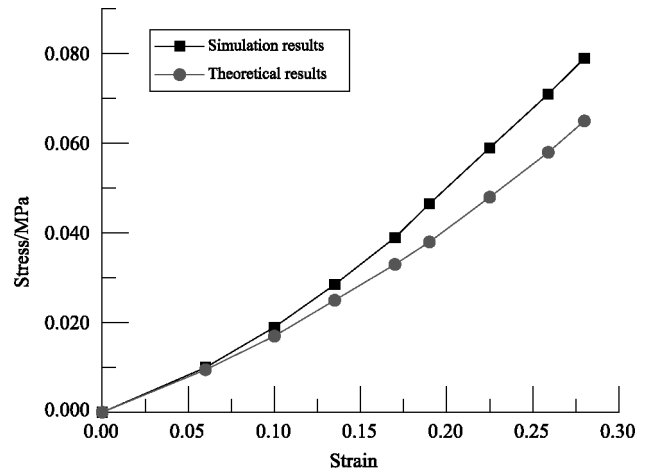


Fig. 8 Stress-strain curve of iliacus

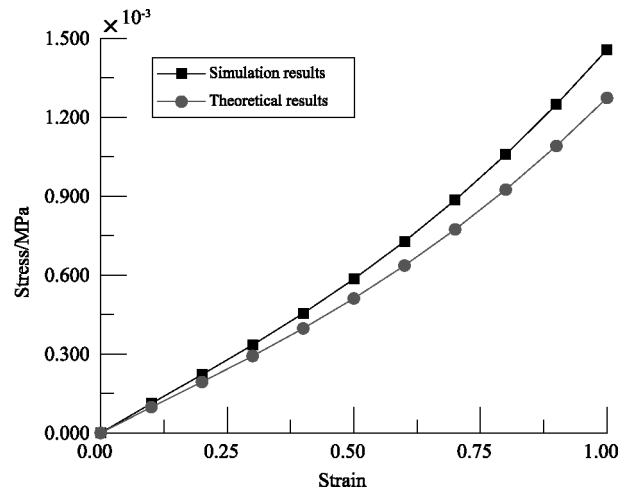


Fig. 9 Stress-strain curve of adipose tissue

### 3.3 Simulation of layered soft tissue deformation

After simultaneously loading 100 N, 200 N, and 300 N on two needles, the simulation results are shown in Fig. 10. The comparison of maximum deformation of pelvic soft tissue under different loads is depicted in Fig. 11.

It can be seen that the deformation is the greatest at the end of the bone needle, while the sacrum exhibits the least deformation. For deformation of circum-pelvic soft tissue; adipose tissue > iliacus muscle > gluteus medius > gluteus maximus. Therefore, the adipose

tissue is more susceptible to damage during loading.

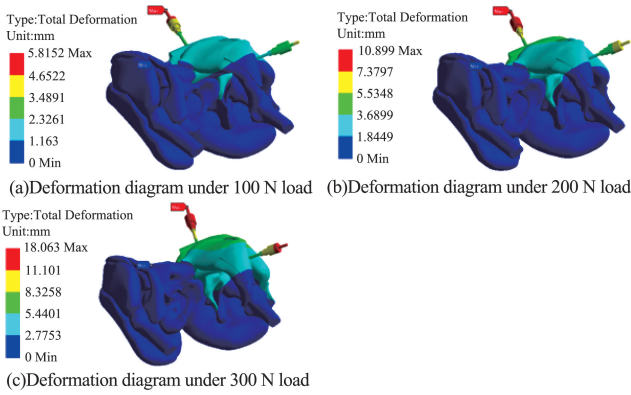


Fig. 10 Simulation results

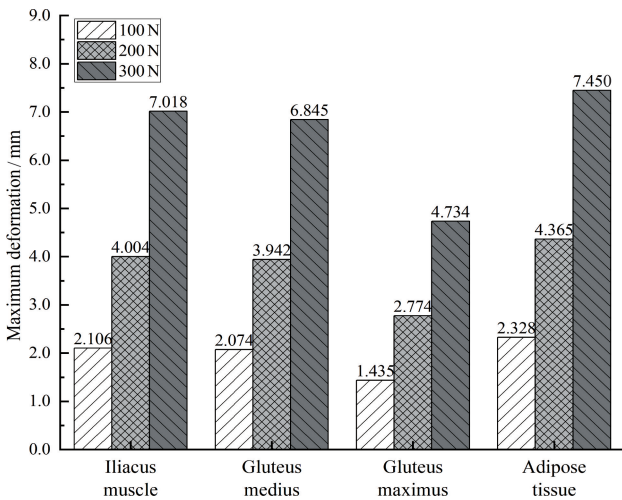


Fig. 11 Maximum deformation of soft tissue

Theoretical calculation and simulation results for the maximum deformation of bone needle are shown in Fig. 12.

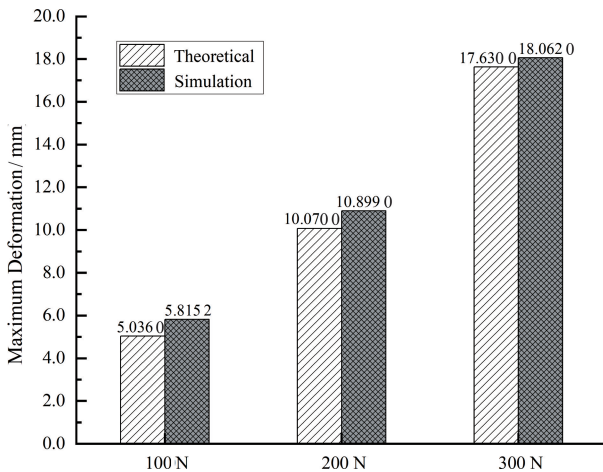


Fig. 12 Deformation results of needle

Under 300 N load, the theoretical calculation and

simulation of maximum needle deformation differ by 0.432 mm, which verifies the correctness of the established needle-tissue interaction model. When the force on the needle increases from 100 N to 200 N, the maximum deformation of needle increases from 5.8152 mm to 10.8990 mm, an increase of 87.42%. When the force is 300 N, the maximum deformation of needle is 18.0620 mm, an increase of 210.60%.

## 4 Conclusions

(1) Considering the layered structural characteristics of soft tissue, a double-layer rigid-flexible coupling model is proposed. The Rayleigh-Ritz method is employed to analyze the interactive deformation of needle-tissue. Under 300 N load, the maximum deformation bone needle is 17.63 mm.

(2) Segregating cortical bone and cancellous bone, distinguishing muscle and adipose tissue, a refined finite element model is established. Adipose tissue deformation is greater than other soft tissue, reaching 7.45 mm under 300 N load.

(3) Verifying the correctness of the established needle-tissue interactive deformation theory analysis, as well as the feasibility of applying it for deformation study of rigid-flexible coupling model. The error between theory and simulation of the maximum needle deformation under 300 N load is 0.432 mm.

## References

- [ 1 ] DIMAIO S P, SALCUDEAN S E. Interactive simulation of needle insertion models [J]. IEEE Transactions on Biomedical Engineering, 2005, 52(7) : 1167-1179.
- [ 2 ] LEHMANN T, ROSSA C, USMANI N, et al. A real-time estimator for needle deflection during insertion into soft tissue based on adaptive modeling of needle-tissue interactions [J]. IEEE/ASME Transactions on Mechatronics, 2016, 21(6) : 2601-2612.
- [ 3 ] LEHMANN T, ROSSA C, USMANI N, et al. Intraoperative tissue Young's modulus identification during needle insertion using a laterally actuated needle [J]. IEEE Transactions on Instrumentation and Measurement, 2017, 67(2) : 371-381.
- [ 4 ] KHADEM M, ROSSA C, USMANI N, et al. A two-body rigid/flexible model of needle steering dynamics in soft tissue [J]. IEEE/ASME Transactions on Mechatronics, 2016, 21(5) : 2352-2364.
- [ 5 ] KHADEM M, FALLAHI B, ROSSA C, et al. A mechanics-based model for simulation and control of flexible needle insertion in soft tissue [C]//2015 IEEE International Conference on Robotics and Automation (ICRA). Seattle, USA : IEEE, 2015 : 2264-2269.
- [ 6 ] YAN K G, PODDER T, YU Y, et al. Flexible needle-tissue interaction modeling with depth-varying mean pa-

- parameter; preliminary study [J]. *IEEE Transactions on Biomedical Engineering*, 2008, 56(2): 255-262.
- [ 7 ] GAO D, LEI Y, LIAN B, et al. Modeling and simulation of flexible needle insertion into soft tissue using modified local constraints [J]. *Journal of Manufacturing Science and Engineering*, 2016, 138(12): 121012.
- [ 8 ] AL-SAFADI S, HUTAPEA P. A study on modeling the deflection of surgical needle during insertion into multi-layer tissues [J]. *Journal of the Mechanical Behavior of Biomedical Materials*, 2023, 146: 106071.
- [ 9 ] TSUMURA R, MIYASHITA T, IWATA H. Mechanical-based model for extra-fine needle tip deflection until breaching of tissue surface [J]. *Journal of Medical and Biological Engineering*, 2018, 38(5): 697-706.
- [10] JUSHIDDI M G, MANI A, SILIEN C, et al. A computational multilayer model to simulate hollow needle insertion into biological porcine liver tissue [J]. *Acta Biomaterialia*, 2021, 136: 389-401.
- [11] PADASDAO B, KONH B. A model to predict deflection of an active tendon-driven notched needle inside soft tissue [J]. *Journal of Engineering and Science in Medical Diagnostics and Therapy*, 2024, 7(1): 011006.
- [12] WEN Y, ZHANG T, YAN W, et al. Mechanical response of porcine hind leg muscles under dynamic tensile loading [J]. *Journal of the Mechanical Behavior of Biomedical Materials*, 2021, 115: 104279.
- [13] JEBUR Q H, JWEEG M J, AL-WAILY M. Ogden model for characterising and simulation of PPHR rubber under different strain rates [J]. *Australian Journal of Mechanical Engineering*, 2023, 21(3): 911-925.
- [14] AL-DIRINI R, REED M P, HU J, et al. Development and validation of a high anatomical fidelity FE model for the buttock and thigh of a seated individual [J]. *Annals of Biomedical Engineering*, 2016, 44(9): 2805-2816.
- [15] SONG H. Finite element analysis and effect observation of external fixator combined with SIJ screw in the treatment of unstable pelvic fracture guided by the principle of balance of bones and muscles [D]. Wuhan: Hubei University of Traditional Chinese Medicine, 2019.
- [16] ZHOU H S, WANG T Y, XU Z, et al. Measurement of the elasticity of biological soft tissue of finite thickness [J]. *Chinese Physics Letters*, 2016, 33(12): 124601.
- [17] LEE H, KIM J. Estimation of flexible needle deflection in layered soft tissues with different elastic moduli [J]. *Medical & Biological Engineering & Computing*, 2014, 52: 729-740.

**ZHANG Famin**, born in 1998. He received his B. S. degree from Zhejiang Sci-Tech University in 2021. Now he is a postgraduate student in School of Mechatronic and Engineering Automation, Shanghai University. His research interest is medical robot.